Published in final edited form as:
IEEE Trans Biomed Eng. 2008 January ; 55(1): 222–229. doi:10.1109/TBME.2007.901039.

A Phased-Array Stimulator System for Studying Planar and Curved Cardiac Activation Wave Fronts

Rashida A. Abbas
Living State Physics Group, Department of Physics and Astronomy, Vanderbilt University, and Division of Cardiovascular Medicine, Vanderbilt University Medical Center, Nashville, TN 37235 USA

Shien Fong Lin
Division of Cardiology, Department of Medicine, Cedars-Sinai Medical Center, and Division of Cardiology, Departments of Medicine and Physiology and Physiological Science, University of California School of Medicine, Los Angeles, CA 90048 USA

David Mashburn
Living State Physics Group, Department of Physics and Astronomy, Vanderbilt University, Nashville, TN 37235 USA

Junkai Xu
Living State Physics Group, Department of Physics and Astronomy, Vanderbilt University, Nashville, TN 37235 USA

John P. Wikswo*

Abstract

Wave front propagation in cardiac tissue is affected greatly by the geometry of the wave front. We describe a computer-controlled stimulator system that creates reproducible wave fronts of a predetermined shape and orientation for the investigation of the effects of wave front geometry. We conducted demonstration experiments on isolated perfused rabbit hearts, which were stained with the voltage-sensitive dye, di-4-ANEPPS. The wave fronts were imaged using a laser and a CCD camera. The stimulator and imaging systems have been used to characterize the relationship between wave front velocity and fiber orientation. This approach has potential applications in investigating curvature effects, testing numerical models of cardiac tissue, and creating complex wave fronts using one-, twoor three-dimensional electrode arrays.

Keywords

Cardiac conduction velocity; Curved activation wavefronts; Multisite stimulation; Tissue anisotropy

I. INTRODUCTION

CARDIAC tissue and other biological and chemical systems that are termed “excitable” can support self-propagating waves. The nonlinear dynamics of these waves has been the subject of intense theoretical and computational investigation, but the corresponding experiments in

*J. P. Wikswo is with the Living State Physics Group, Department of Physics and Astronomy, and Departments of Biomedical Engineering, Molecular Physiology & Biophysics, Vanderbilt University, Nashville, TN 37235 USA (e-mail: john.wikswo@vanderbilt.edu)..

general utilize only a limited number of experimental stimulation protocols. Because cardiac wave fronts exhibit a curvature-dependent velocity, the shape of the wave front affects its propagation and hence plays a role in the generation and stability of cardiac arrhythmias. A difference in conduction velocity has been observed between the planar wave fronts created by a linear array of electrodes and the curved wave fronts produced by point stimulation [1; 2] Wave fronts of varying curvature created by conduction through an isthmus of varying width have shown a similar effect of curvature on conduction velocity [3;4]. Also, a recent study demonstrates an inverse relation between wave front curvature and velocity in reentrant circuits that cause ventricular tachycardia [5]. Along with curvature, it is well known that as a result of the anisotropy of the electrical conductivity of cardiac tissue, the propagation velocity of a wave front depends upon the direction of propagation, traveling faster along the direction of the tissue fibers than in the perpendicular direction [6;7]. In the intact whole heart the direction of the fiber axis changes with depth from the epicardial surface to the endocardium [8], further complicating wave front dynamics [9;10].

In a simple model of anisotropic conduction in excitable media, propagation velocity is a function of the angle between the fiber axis and the normal to the propagating wave front and is described by [11;12]

$$v(\phi) = \left[(v_l \cos\phi)^2 + (v_t \sin\phi)^2 \right]^{1/2}, \quad (1)$$

where v_l is the velocity of a planar wavefront propagating in a direction parallel to the fiber axis, v_t is the velocity in the direction transverse to the fiber axis and ϕ is the angle between fiber axis and the normal to the wave front. The experimental validation of Equation (1) is not yet complete and would benefit from improved methods for generating plane waves of an arbitrary orientation. A quantitative study of the dependence of conduction velocity on the angle of the wave front relative to the fiber direction is best conducted through the creation of planar wave fronts, to eliminate the contribution of curvature effects.

We describe a phased-array stimulator system that enables the spatiotemporally complex stimulation protocols that will allow us to the study the characteristics of wave front propagation in cardiac tissue. The stimulator uses an array of small stimulating electrodes to create wave fronts of tissue activation of a desired shape and orientation. An epifluorescence imaging system with a voltage sensitive dye, laser illumination, and a charge-coupled device camera are used to image the wave front propagation.

The concept of phased-array stimulation has been taken from the field of phased-array radar, which uses multiple transmitters and phase control to direct a radar beam at some angle in space by using a Huygens reconstruction of a wave front from a linear array of point sources producing expanding circular waves [13-15]. The characteristics and angle of the beam are modified through independent control of the amplitude and phase of each transmitter. We applied this method to cardiac tissue by using multiple unipolar point stimulators, with independently controlled timing and amplitude applied at various locations over the surface of a heart in order to create wave fronts of predetermined shape and orientation. As shown in Figure 1A, a single pointstimulating electrode in cardiac tissue creates an expanding wave front of activation that can be approximated by an ellipse (Figure 1B) whose major axis is parallel to the tissue fiber axis. Consistent with a Huygens reconstruction, the two plane wave fronts in Figure 2 can be approximated by the envelope of the elliptical wave fronts produced by multiple stimuli delivered at different locations. Notably, these colliding wave fronts produce regions of high curvature near the area of intersection, allowing the creation of curved wave fronts as well as simple linear wave fronts.

The phased-array system is well suited to create planar and curved wave fronts for the study of wave front dynamics in cardiac tissue, by using phase and amplitude control of multiple stimulating electrodes. In theory, this may be done using the approach described above; however, due to the large number of parameters that must be adjusted, this is difficult to execute without computer automation. To achieve this, we have devised a software emulator of the stimulator hardware that calculates stimulator parameters for a desired geometry. These parameters are then used to control the timing and amplitude of the hardware stimulator, and to synchronize stimulator timing with that of image acquisition.

II. INSTRUMENTS DESCRIPTION

A. Device Overview

We have produced two implementations of the device, the first using on-board, remotely programmed microcontrollers for the timing, and the second using a timing board in a microcomputer workstation. We will describe the first implementation in detail, and then summarize the changes for the second implementation.

The phased-array stimulator consists of a LabView™ driven emulator that is used to compute the desired stimulus timing, a digitally-controlled hardware stimulator with thirty individually programmable channels, and an argon laser and a CCD camera for fluorescence imaging. Figure 3 shows an overview of the phased-array stimulator and an early implementation of the optical recording system [16]. The operator first selects the orientation of the desired planar wave front to be created, and specifies the parameters into the LabView™ emulator. The emulator then calculates the necessary timing required at each stimulation electrode to create the wave front. The operator may, if desired, adjust the timing and amplitude of each of the channels prior to implementation. The parameters are then downloaded into the stimulator, which controls image acquisition synchronously with the stimulation sequence (Figure 4). The activation wave front is extracted from the raw fluorescence images, and wave front propagation velocities are calculated using custom Matlab™ image processing algorithms.

B. Software Emulator

The software emulator, implemented in LabView™, provides a numerical representation of thirty electrodes arranged in a circle around an imaging area. Prior to setting up the emulator, a point stimulus at the center of the imaging window is applied to the real tissue, and an optical measurement of the resulting expanding wave front, as shown in Figure 1, is used to determine the fiber direction (the major axis of the ellipse). Since the expansion of the ellipse reflects the longitudinal and transverse velocities associated with the heart being studied, for the emulator we chose to begin with velocities that were taken from our measurements. The next step towards emulating the creation of a planar wave front is to choose the desired orientation of the wave front, which is input into the software emulator in terms of the slope of a line. Given this line, it is then necessary to determine the delays between each of the stimuli whose Huygens' wavelets will be superposed to form the complete wave front. To vary the shape of the final wave front, we can subsequently adjust the delay of each stimulus independently. The emulator calculated the timing as explained in the following:

An ellipse centered at the origin, with semi-minor axis a and semi-major axis b, is described in polar coordinates r and β by

$$\{r(\beta)\}^2 = \frac{a^2 b^2}{a^2 \sin^2\beta + b^2 \cos^2\beta}, \tag{2}$$

where β is the angle parameter for the ellipse relative to the semi-major axis. If the ellipse expands with fixed velocities in the longitudinal and transverse directions, given by v_l and v_t, respectively, then the parameters *a* and *b* are described as functions of time by

$$a=v_l t \quad \text{and} \quad b=v_t t \tag{3}$$

Equation (2) then becomes:

$$r=v_l v_t\left[v_l^2\sin^2\beta+v_t^2\cos^2\beta\right]^{-1/2}t. \tag{4}$$

For a single stimulus applied to the center of the imaging field of the camera, the resulting expanding wave front is an ellipse centered at the origin, with semi-major axis at angle θ with the *x* axis. The ellipse is then described by

$$r=v_l v_t\left[v_l^2\sin^2(\beta+\theta)+v_t^2\cos^2(\beta+\theta)\right]^{-1/2}t, \tag{5}$$

where θ is the angle between the tissue fiber direction and the *x* axis of the image (hereafter we use *x* and *y* to describe the camera axes). The elliptical wave front created at each point in the stimulator array is emulated by translating the center of the expanding ellipse given by Equation (5) to the edge of a circle of radius *R* (representing the imaging window) at angle α. The major axis of the ellipse will be at angle θ with the *x* axis. The delay used by the emulator is the time *t* at which the ellipse intersects the edge of the specified wave front represented by the dashed line in Figure 5.

The predicted ellipses and the resulting planar front are plotted in the emulator and the emulated wave front is allowed to propagate over time. Multiple wave front orientations can be emulated prior to activating the hardware stimulator, at which point the calculated delays are automatically loaded into the stimulator front panel. After this step, the operator can, if desired, further adjust either the delay or amplitude of each channel prior to beginning the stimulation sequence. Wave fronts with regions of varying degrees of high negative curvature can also be created by the collision of two planar wave fronts.

C. Hardware Stimulator

We have developed two implementations of the device. The first has dedicated timing circuits, requires only a minimal low data-rate computer interface for serial preprogramming of the timers, and is suitable for implementation as a stand-alone device. The second is simpler electronically but is significantly more expensive because it requires a high-speed workstation and multichannel digital and analog control cards, and relies on fast software to control the entire device in real time. The preference for one over the other would be determined in part by the user's particular application, budget, electronics capabilities, and computer resources.

The first implementation of the stimulator used an array of AM9513 (Advanced Microdevices) programmable timing chips. After the timing parameters obtained from the simulation as described previously are adjusted and felt to be satisfactory, they are automatically loaded into the LabView™ nprogram controlling the stimulator. The stimulator control front panel (shown in Figure 4) allows the user to further adjust each of the thirty delays and amplitudes prior to tissue stimulation. The AM9513 timing chips are programmed using the LabView™ emulator and a LABNB data acquisition board installed in a Macintosh. The stimulator consists of thirty

optically isolated channels with stimulus amplitude controlled by the same LABNB board via input from the LabView™ stimulator control panel.

While the AM9513 microcontroller approach of Figure 6 has the advantage of stand-alone operation, it has the disadvantages of electronic complexity and the need to download the required timing sequences. Hence this system is not suitable for real-time control of wave fronts. To address this limitation, we have created a second implementation of the device wherein the voltages required to program the current sources are provided continuously by a 32-channel digital-to-analog converter (National Instruments PCI-6723), and the digital control of the pulse timing is provided by a digital pattern I/O card (National Instruments PCI-6534). Figure 7 shows an overview of the stimulation control of the system. The new LabView™ program serves as our user interface, which takes information from the operator and calculates the timing information, then transfers the data to the two PCI cards. These, in turn, are connected to the backplane of the stimulator chassis, which further routes the signals to individual channels on the current source boards. The stimulator chassis contains four custom, voltage-driven current source boards, each with 8 optically isolated, digitally switched channels. Figure 6 shows the original circuit which uses a sample-and-hold, followed by an opamp buffer, a digital switch, an optoisolator, a second buffer, and then a resistive current source with a transistor amplifier. In order to maintain electrical isolation, the first half of the circuit is powered by a solid-state supply, and the optically isolated second half is powered by a high-capacity battery. The positive pole of the battery is connected to the spiral return electrode that is pressed against the back of the heart to complete the circuit. The boards from the second implementation differ from those in the first implementation (Figure 6) by having each stimulator channel receive a constant control voltage from thePCI-6723 card, rather than a control voltage that is loaded serially and stored in a sampleand-hold capacitor. In operation, the stimulator delivers constant-current pulses (*i.e.*, square) with given duration (typically 2 ms) and amplitude (typically twice the threshold level) to each of a maximum of thirty-two electrodes on the heart's surface. A separate version of the LabView™ emulator controls the amplitude and timing of these pulses. The digital card has 64 Mbyte on-board memory, permitting the storage of a sequence of stimuli of up to 16 seconds in duration with a timing resolution of 1 μs. As in the first implementation, the LabView™ emulator also allows easy adjustment of the stimulus strength and inter-channel delays to optimize the shape of the resulting propagating wave front.

D. Imaging System

The imaging system uses a cooled CCD camera with a 50 mm f1.8 objective lens and a 5 W argon laser, as described in detail elsewhere [16]. An acousto-optic modulator (AOM) was used to strobe the laser illumination of the heart to provide a shorter effective exposure time than would be possible with the intrinsic shutter speed of the camera. Less blurring of the wave front edge due to propagation is thus achieved with an effective exposure time of 0.5 ms. Camera shutter timing and AOM (acousto-optic modulator) were controlled using a timing device (TIO) installed in a Macintosh computer. Integration between stimulator, camera and laser timing is achieved using LabView™ control of both the stimulator system and the TIO device. An external pulse generator served as the trigger for both the TIO and the stimulator-timing device, and synchronized image acquisition with stimulator output.

To acquire a sequence of 100 × 100 pixel images of a 7.5 × 7.5 mm field of view on the heart separated by intervals of 1 to 3 ms, we used 3 × 3 binning of a 300 × 300 pixel region and boxcar signal averaging for signal-to-noise enhancement [16].

EXPERIMENTAL METHODS AND RESULTS—To demonstrate phased-array stimulation, we performed experiments on the anterior left ventricle of isolated Langendorff-

perfused New Zealand rabbit hearts. All experiments were conducted in accordance with National Institutes of Health regulations for the ethical use of animals in research and were approved in advance by the Vanderbilt Institutional Animal Care and Use Committee. New Zealand rabbits were anesthetized with IM ketamine and intravenous sodium pentobarbital. We removed the hearts quickly, mounted them on a Langendorff apparatus and perfused them with Tyrode's solution, which was oxygenated and maintained at 37 - 38 oC. Hearts were stained with the voltage sensitive dye di-4-ANEPPS and an electromechanical decoupler, diacetyl monoxime (15 mM), was added to the perfusate to inhibit muscle contraction [17; 18].

Against the surface of the heart, we placed an imaging window that consisted of a circular 12.5 mm hole in a plexiglass plate with unipolar stimulating electrodes equally spaced at the edge of the window (Figure 8). Silver wire wound into a 1 cm diameter planar spiral and placed in contact with the posterior surface of the heart functioned as the return electrode. Point stimulation at a site in the center of the imaging window was provided by a removable 100 μm diameter insulated platinum wire with an insulation-free central kink, which contacted the surface of the heart.

Fiber orientation was initially determined by observing the major axis of the elliptical region of activation created by point stimulation at the center of the imaging window. A series of plane waves at various orientations relative to fiber direction were emulated, the timing sequences were downloaded to the stimulator, and the conduction velocities for the wave fronts were calculated using the procedure described subsequently. In general, only minimal adjustments to the stimulator timing, relative to the timing parameters derived from the simulations, were required to create the plane wave. This supports the assumption that activation patterns obtained during the observed time sequence (up to 18 ms) reflect predominantly epicardial activation and therefore predominantly epicardial fiber orientation.

Image processing: From the raw epifluorescence images, we followed a series of image processing steps developed using MatlabTM, as outlined in Figure 9. From these, we produced the wave front images and the wave front conduction velocities. To correct for variations in fluorescence due to tissue inhomogeneities, we used the standard practice of dividing the value of each pixel by the average background value associated with that pixel. The background value of a pixel is the average over a selected time interval for that pixel during which the tissue is at rest. We found the direction of the tissue fibers relative to the camera axes by imaging the expanding ellipse of depolarized tissue that followed stimulation of the tissue with a point electrode placed at the center of our electrode array. The fiber direction was measured as the direction of a manually estimated line passing through the major axis of the image of this ellipse with respect to the camera coordinates. We used thresholding at half the maximum fluorescence change to convert the planar wave front image to binary (1 or 0) and then extracted the wave front edge from the resulting black and white image. We calculated the planar wave front conduction velocities as a function of angle with the fiber direction from a series of best-fit lines over a sequence of images. We fit the wave front edge to a straight line and calculated the angle between the wave front edge and the myocardial fiber direction. At six points along the best-fit line for each wave front at time t, we measured the distance between this wave front and the subsequently propagated wave front (at time t + 1) along the normal to the first wave front at each point. The average of these distances was used to obtain the conduction velocity for each plane wave.

The second panel in Figure 9 shows images obtained after the initial image processing steps just described for the propagation of a plane wave across the field of view. The light regions correspond to depolarized, or activated tissue, and the dark regions correspond to resting tissue. Each block in the panel shows the same 7.5 × 7.5 mm region of the tissue at 3 ms increments

of time after stimulation. Figure 10 shows several of the planar wave fronts created using phased array stimulation. Each panel shows a time sequence associated with a propagating wave front originating from the (A) top of the imaging window, (B) right, and (C) left. Panel (D) shows the wave front resulting from the collision of two planar wave fronts. Figure 11 shows the results of several stimulation protocols. Panel (A) shows fiber direction as determined by the major axis of the elliptical region of activation resulting from central point stimulation. Panels (B) and (C) show plane waves from the same region of the heart, with calculated conduction velocities.

DISCUSSION—Optical imaging systems have been widely applied to the study of cardiac tissue activation and propagation, including preliminary investigations of the velocity-curvature relationship and the demonstration of differences in transverse versus longitudinal conduction velocities. The system we have described here allows the creation of wave fronts of a desired shape and orientation by means of programmable stimulus timing, using a Huygens construction to estimate the necessary timing of each of the multiple stimuli. The technique has potential applications in quantitative studies of the characteristics of cardiac tissue activation. One such characteristic is the dependence of conduction velocity on direction. We have used this system to create planar wave fronts at multiple angles relative to tissue fiber direction. We have implemented an image processing procedure that uses thresholding, edge extraction, and line-fitting to measure plane wave conduction velocities. Conduction velocities are being measured from the analysis of pooled data from approximately fifteen experiments. This system would be suitable for control of the stimulus timing for any configuration of electrodes. For example, a linear array in a plunge electrode could be used to produce a wave front that progressed radially through the myocardial wall. An array of such electrodes could produce even more complicated wave fronts [19].

The influence of fiber rotation within the myocardium on the propagation of wave fronts originating from the epicardium in the intact ventricle is an area of current investigation. Recently, a method has been described for investigating the direction of wave front propagation in subepicardial layers resulting from epicardial stimulation [20;21]. This method makes use of the observation that the action potential recorded by optical imaging at the epicardium, using voltage sensitive dyes, represents the average action potential created by a volume of multiple myocytes. For epicardial stimulation, as in our experiments, shortly after stimulation, the wave front should reflect predominantly epicardial fiber orientation. Subsequently, the propagated wave fronts would be expected to have a greater contribution from the activation of layers deeper within the myocardium. The extent to which these phenomena affect the control and response of phased-array stimulation has yet to be determined.

As compared to planar wave fronts, wave fronts with negative curvature (i.e., concave) are predicted to propagate with a greater velocity, and convex or positively curved wave fronts propagate with a lesser velocity. We have observed wave fronts of varying degrees of high negative curvature created through the collision of planar wave fronts, and we are in the process of developing similar image processing techniques for the measurement of curvature and its effects on velocity.

III. CONCLUSION

Models that attempt to explain the nature of the electrical properties of cardiac tissue are continually evolving. We believe that phased array stimulation is a useful tool for the experimental validation of emerging models through the quantitative study of their predictions. The ability to create controllable wave fronts coupled with fluorescence imaging is well suited to the study of wave front dynamics, and can enhance our understanding of the behavior of propagating wave fronts in cardiac tissue.

Acknowledgments

This work has been supported in part by the National Institutes of Health Grant R01-HL58241-05 and the Vanderbilt Institute for Integrative Biosystems Research and Education.

Biographies

Rashida Abbas received the B.S. degree in physics from Drexel University in Philadelphia, PA and the M.D. degree from the University of Pennsylvania in Philadelphia, PA. She received the M.S. degree in physics and completed her residency in Internal Medicine at Vanderbilt University in Nashville, TN. She is currently a fellow in Cardiovascular Medicine at Vanderbilt. Her research interests are in the area of electrophysiology and mechanisms of arrhythmia, including the study of wave front dynamics in cardiac tissue using optical imaging techniques.

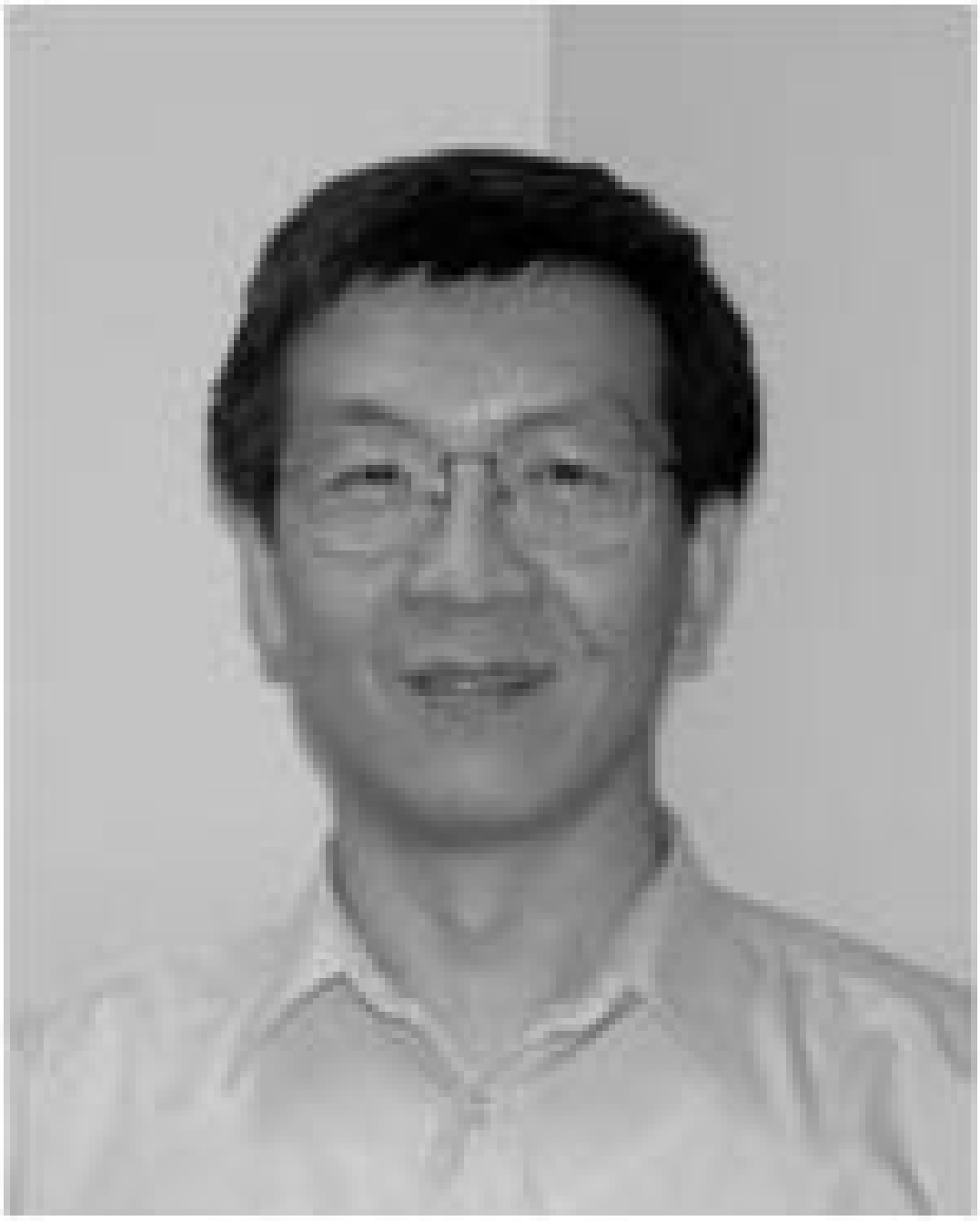

Shien-Fong Lin received the B.S. degree in Communication Engineering from National ChiaoTung University in Taiwan, and M.S. and PhD degrees in Biomedical Engineering from Northwestern University in Evanston, IL. He joined the Living State Physics Group at Vanderbilt University in 1992 and pioneered cardiac optical mapping technique to measure electrical excitation and propagation in cardiac tissue. He won the first prize in the Young Investigator Competition in North American Society of Pacing and Electrophysiology in 1998. In 2001, he joined the Electrophysiology Research Group in Cedars-Sinai Medical Center in Los Angeles, CA. He is now an Associate Professor at David Geffen School of Medicine in UCLA. His research interests include cardiac electrophysiology, control of arrhythmias, biomedical optics and biomedical image processing.

David Mashburn is pursuing his Ph. D. in Physics at Vanderbilt University, Nashville, TN. He graduated summa cum laude from Vanderbilt with a B.S. in Physics and Mathematics in 2006. His research interests include cardiac wavefront geometry and dynamics and cardiac activation patterns in defibrillation shocks; his research involves modeling and experiments.

John P. Wikswo (M'75-SM'05) received the B.A. degree in physics from the University of Virginia, Charlottesville, and the M.S. and Ph.D. degrees in physics from Stanford University, Stanford, CA. He was a Research Fellow in Cardiology at the Stanford University School of Medicine from 1975 to 1977. He joined the faculty in the Department of Physics and Astronomy at Vanderbilt University, Nashville, TN, as an Assistant Professor of Physics in 1977. He is now the Gordon A. Cain University Professor, A.B. Learned Professor of Living State Physics, Director of the Vanderbilt Institute for Integrative Biosystems Research and Education (VIIBRE), and Professor of Biomedical Engineering, Molecular Physiology and Biophysics, and Physics. He has been a Woodrow Wilson Fellow, an NSF Predoctoral Fellow, an Alfred P. Sloan Research Fellow, and a John Simon Guggenheim Fellow. At Vanderbilt,

his research has been directed primarily towards using novel instrumentation, electric and magnetic measurements, and electromagnetic theory for studying the propagation of bioelectric activity, nondestructive testing, and biological microelectromechanical systems (BioMEMS). He has taken an active role in arguing that judicial electrocution constitutes cruel and unusual punishment. His current research includes studies of the role of tissue anisotropy on the initiation and propagation of cardiac action potentials, and the application of cellular instrumentation and control to experimental systems biology.

Dr. Wikswo is a fellow of the American Physical Society, the American Institute for Medical and Biological Engineering, the American Heart Association, the Council on Basic Cardiovascular Sciences of the American Heart Association, the Biomedical Engineering Society and the Heart Rhythm Society.

Junkai Xu received the B.S. degree in biophysics from Nanjing University, Nanjing, Jiangsu, China in 2001. He is now a graduate student in the Department of Physics at Vanderbilt University, Nashville, TN. He is expecting his PhD degree in Physics in August 2007. His research includes studying the mechanism of cardiac wave propagation by observing the electric activity on heart surface and developing novel instrumentation to facilitate that research. Most recently his research involves development of an ultra-sensitive nanocalorimeter which can be used to measure cell metabolism and it's variation under change of physical/chemical environment such as injections of toxin.

REFERENCES

[1]. Knisley SB, Hill BC. Effects of Bipolar Point and Line Stimulation in Anisotropic Rabbit Epicardium: Assessment of the Critical Radius of Curvature for Longitudinal Block. IEEE Trans. Biomed. Eng 1995;42(10):957–966. [PubMed: 8582725]

[2]. Cabo C, Pertsov AM, Baxter WT, Davidenko JM, Gray RA, Jalife J. Wave-Front Curvature as a Cause of Slow Conduction and Block in Isolated Cardiac Muscle. Circ. Res 1994;75:1014–1028. [PubMed: 7525101]

[3]. Fast VG, Kleber A. Block of impulse propagation at an abrupt tissue expansion: evaluation of the critical strand diameter in 2- and 3-dimensional computer models. Cardiovasc. Res Sept;1995 30 (3):449–459. [PubMed: 7585837]

[4]. Fast VG, Kleber AG. Cardiac tissue geometry as a determinant of unidirectional conduction block - assessment of microscopic excitation spread by optical mapping in patterned cell-cultures and in a computer-model. Cardiovasc. Res 1995;29(5):697–707. [PubMed: 7606760]

[5]. Chow AWC, Schilling RJ, Davies DW, Peters NS. Characteristics of Wavefront Propagation in Reentrant Circuits Causing Human Ventricular Tachycardia. Circulation May;2002 105(18):2172–2178. [PubMed: 11994251]

[6]. Spach MS, Miller WT III, Geselowitz DB, Barr RC, Kootsey JM, Johnson EA. The Discontinuous Nature of Propagation in Normal Canine Cardiac Muscle. Circ. Res 1981;48(1):39–54. [PubMed: 7438345]

[7]. Corbin LV II, Scher AM. The canine heart as an electrocardiographic generator. Dependence on cardiac cell orientation. Circ. Res 1977;41(1):58–67. [PubMed: 862144]

[8]. Streeter DD, Ramon C. Muscle Pathway Geometry in the Heart Wall. J. Biomech. Eng 1983;105:367–373. [PubMed: 6645446]

[9]. Muzikant AL, Hsu EW, Wolf PD, Henriquez CS. Region specific modeling of cardiac muscle: Comparison of simulated and experimental potentials. Ann. Biomed. Eng 2002;30(7):867–883. [PubMed: 12398418]

[10]. Muzikant AL, Henriquez CS. Validation of three-dimensional conduction models using experimental mapping: are we getting closer? Prog. Biophys. Mol. Biol 1998;69:205–223. [PubMed: 9785939]

[11]. Muler AL, Markin VS. Electrical Properties of Anisotropic Nerve-Muscle Syncytia - II. Spread of Flat Front of Excitation. Biofizika 1977;22(3):518–522. [PubMed: 889914]

[12]. Roberts DE, Hersh LT, Scher AM. Influence of cardiac fiber orientation on wavefront voltage, conduction velocity, and tissue resistivity in the dog. Circ. Res 1979;44(5):701–712. [PubMed: 428066]

[13]. Fenn AJ, Temme DH, Delaney WP, Courtney WE. The development of phased-array radar technology. Lincoln Laboratory Journal 2000;12(2):321–340.

[14]. Hecht, E. Optics. Addison-Wesley; 1979. Reading etc

[15]. Mailloux RJ. Phased-Array Theory and Technology. Proc. IEEE 1982;70(3):246–291.

[16]. Lin S-F, Abbas RA, Wikswo JP Jr. High-resolution High-speed Synchronous Epifluorescence Imaging of Cardiac Activation. Rev. Sci. Instrum 1997;68(1):213–217.

[17]. Li T, Sperelakis N, Teneick RE, Solaro RJ. Effects of diacetyl monoxime on cardiac excitation-contraction coupling. J. Pharmacol. Exp. Ther Mar;1985 232(3):688–695. [PubMed: 3156242]

[18]. Baker LC, Wolk R, Choi BR, Watkins S, Plan P, Shah A, Salama G. Effects of mechanical uncouplers, diacetyl monoxime, and cytochalasin-D on the electrophysiology of perfused mouse hearts. Am. J. Physiol. Heart Oct;2004 287(4):H1771–H1779.

[19]. Frazier DW, Krassowska W, Chen P-S, Wolf PD, Danieley ND, Smith WM, Ideker RE. Transmural Activations and Stimulus Potentials in Three-Dimensional Anisotropic Canine Myocardium. Circ. Res 1988;63:135–146. [PubMed: 3383372]

[20]. Hyatt CJ, Mironov SF, Vetter FJ, Zemlin CW, Pertsov AM. Optical Action Potential Upstroke Morphology Reveals Near-Surface Transmural Propagation Direction. Circ. Res Aug;2005 97(3): 277–284. [PubMed: 15994436]

[21]. Kleber AG. The Shape of the Electrical Action-Potential Upstroke: A New Aspect From Optical Measurements on the Surface of the Heart. Circ. Res Aug;2005 97(3):204–206. [PubMed: 16081874]

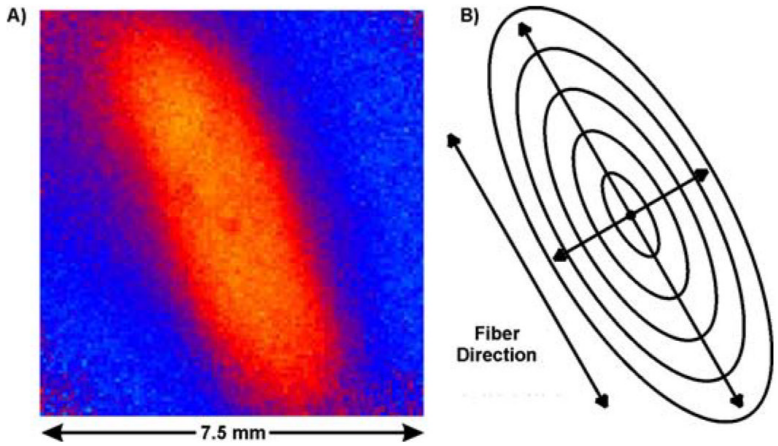

Fig. 1.

The wave fronts propagating from a point stimulus applied to cardiac tissue. A) Optical fluorescence measurement of the transmembrane voltage distribution, showing the outer edge, or wave front, of the expanding region of depolarization at one time instant. B) Schematic representation of the equivalent expanding ellipses.

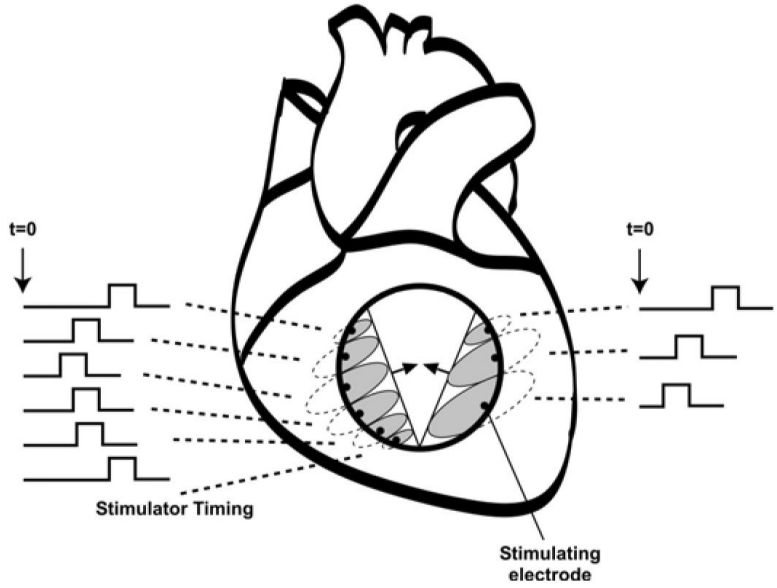

Fig. 2.

A schematic illustration of the heart and the imaging window that supports the circular array of stimulus electrodes. Each ellipse represents the wave front created by a point stimulus at the center of the ellipse, at the edge of the circular window. The arrows represent the direction of propagation. The pulses outside the window show the timing of the various stimuli that would be used to create the Huygens wave fronts that merge to form the pair of colliding wave fronts shown within the window.

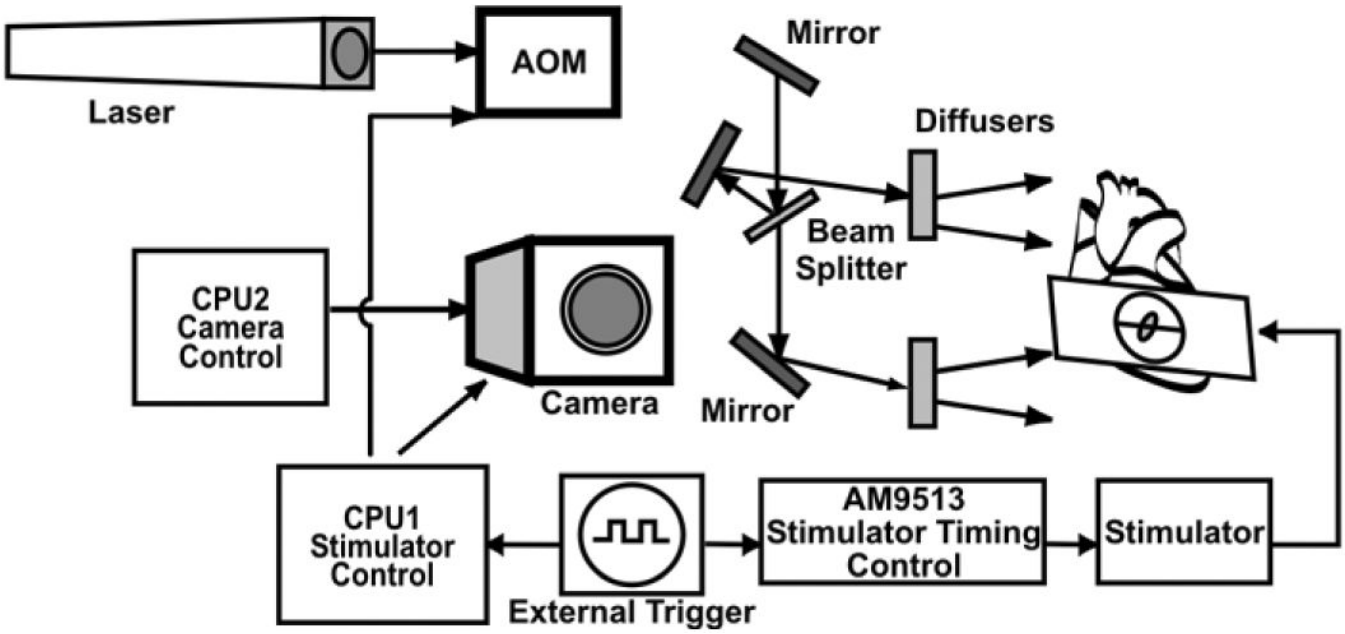

Fig. 3.
A block diagram showing the components of the phased-array stimulator and cardiac imaging systems. (AOM = Acoustooptic modulator)

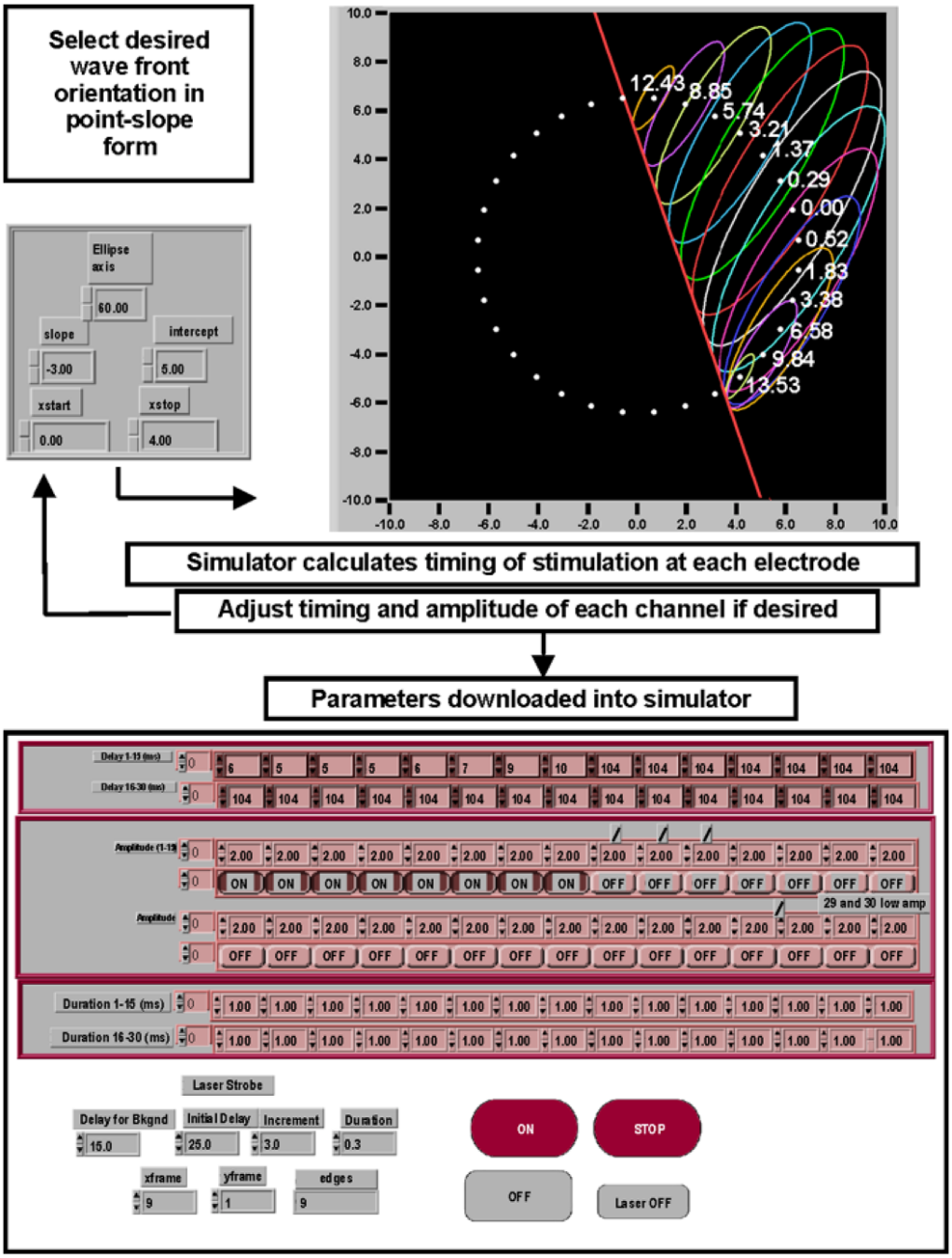

Fig. 4.

A schematic of the steps that are followed within the LabView™ program to emulate the desired wave front geometry. The LabView™ front panel is shown. The numbers in the emulation plot represent the time in milliseconds after the first electrode is fixed.

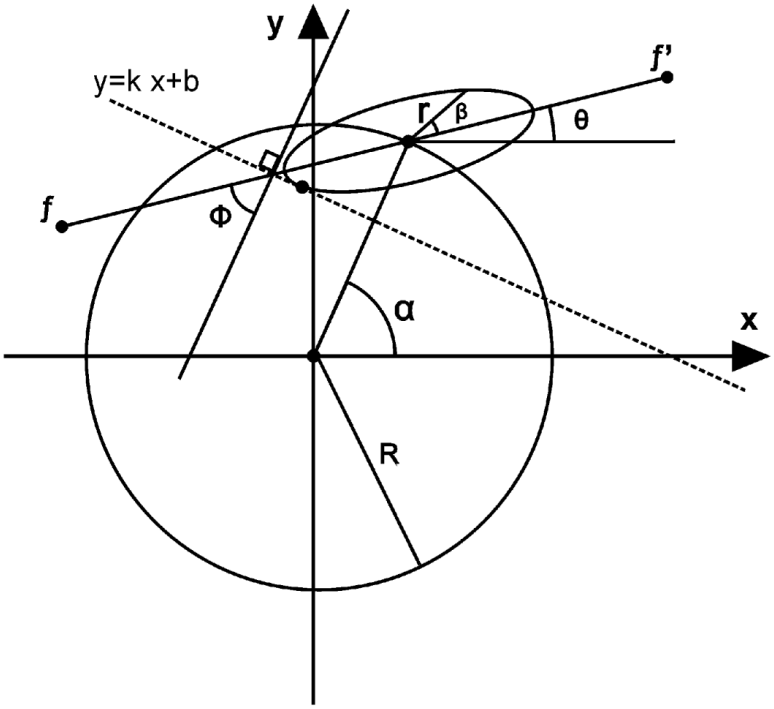

Fig. 5.

The geometry used in computing the Huygens reconstruction and the stimulus timing, where *x* and *y* are the camera axes, and line [*f*,*f*'] identifies the cardiac fiber axis.

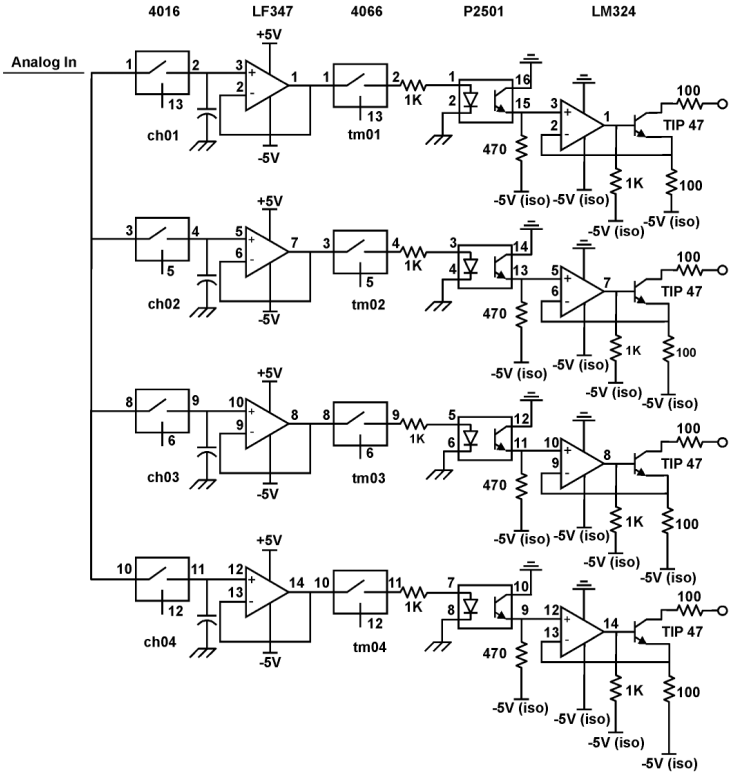

Fig. 6.

Circuit diagram for the first implementation of the stimulator. Only four of the channels are shown. ch01-4 are the digital lines that control which capacitor is to receive voltage-setting from the analog line. tm01-4 are the digital lines that control the firing of individual channels. “(iso)” refers to the isolated power supply (battery).

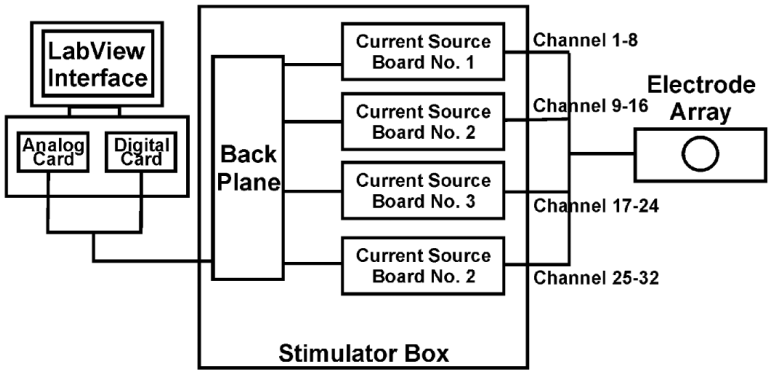

Fig. 7.
Block diagrams for the second implementation of the stimulator.

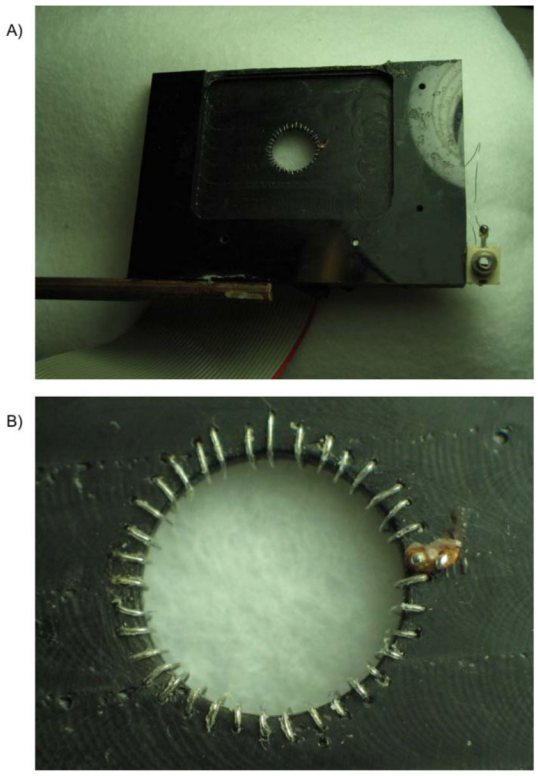

Fig. 8.
Imaging window and stimulator array. A) shows the surface of the plexiglass plate which stays in contact with the heart, and the stimulator array around the edges of the circular imaging window. B) A close-up view of insulated platinum wire stimulating electrodes with insulation-free region contacting the surface of the heart.

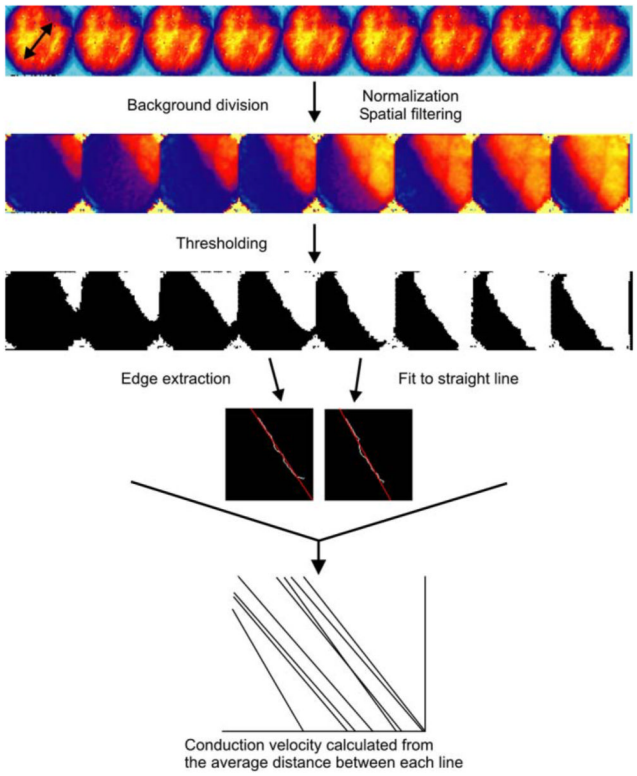

Fig. 9.
Overview of the image processing steps used to determine plane-wave conduction velocities. The arrow in first frame shows fiber direction.

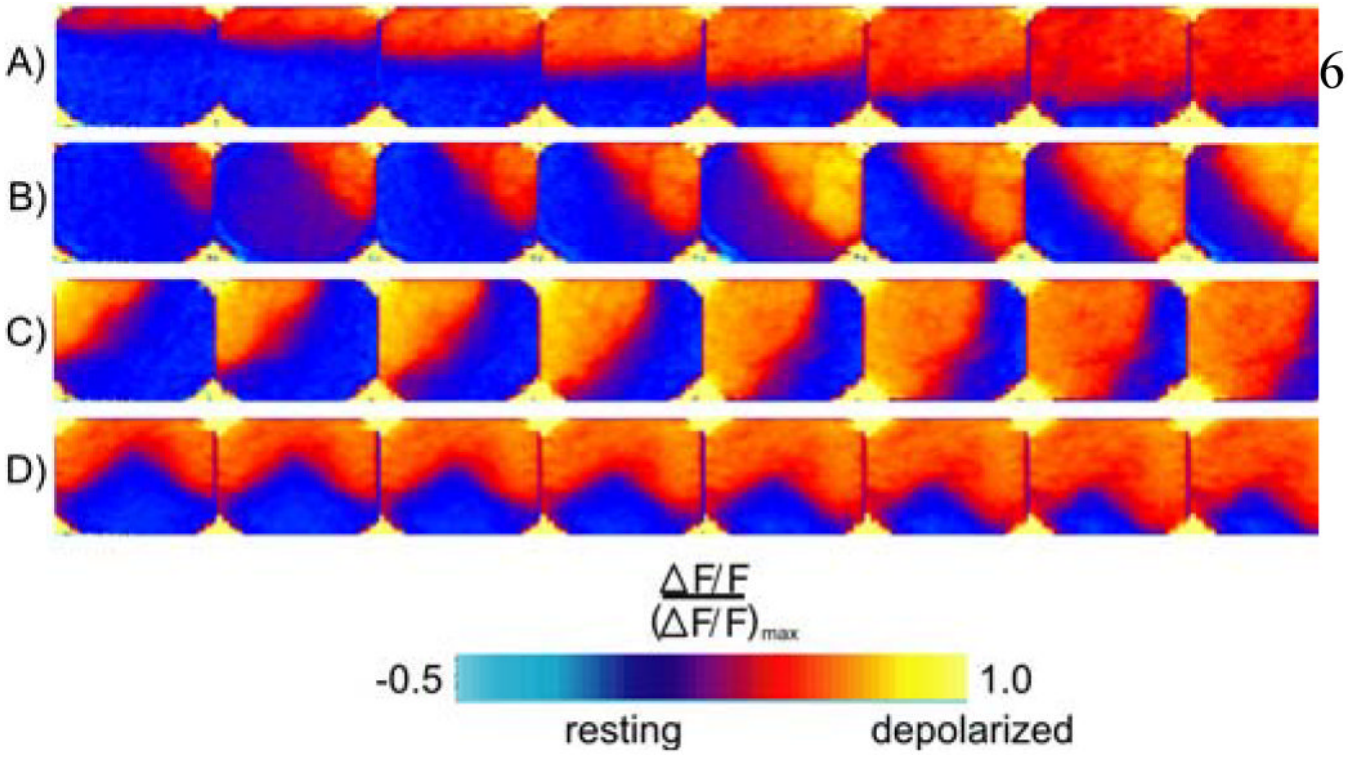

Fig. 10.

Plane waves created using various phased array stimulation parameters. Δ*F*/*F* is the fractional change in fluorescence, which is proportional to the change in transmembrane potential and is expressed as a percentage of the maximal change. Values of zero and one correspond to resting and maximally depolarized tissue, respectively. The arrow in panel A) shows fiber direction.

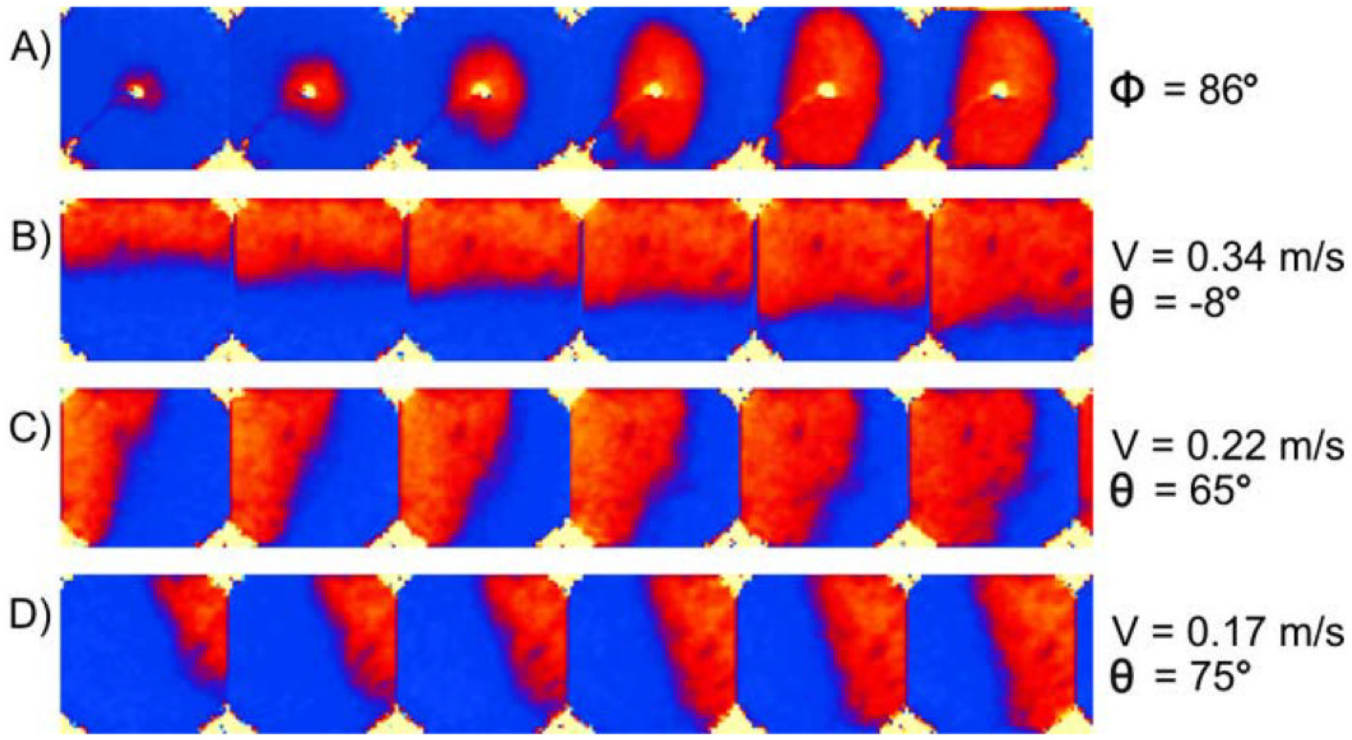

Fig. 11.
Plane waves created using several stimulation protocols. A) Fiber direction relative to the horizontal axis. B-D) show plane waves from the same region of the heart, with calculated conduction velocities and angles relative to fiber direction.